

Direction Cosine Matrix Estimation with An Inertial Measurement Unit

Yan Wang^a, Rajesh Rajamani^a

^a*Department of Mechanical Engineering, University of Minnesota, Minneapolis, MN 55455, USA*

Abstract

Estimating attitude using an inexpensive MEMS inertial measurement unit has many applications in smart phones, wearable sensors, rehabilitation medicine and robots. Traditional approaches to attitude estimation from the aerospace world focus on the use of either Euler angles or quaternions. These approaches suffer from disadvantages including singularities and nonlinear models. This paper proposes a method to estimate the direction cosine matrix (DCM) which encapsulates attitude information, instead of Euler angles or quaternions. The DCM does not suffer from singularities and also has linear dynamics. A rigorous DCM estimation algorithm, that incorporates automatic magnetometer bias calibration and satisfaction of an inherent orthonormal property of the DCM, is developed. The validity of the developed algorithm is demonstrated through experimental results with estimation of attitude on a 5-DOF robot. The estimation results are compared with values computed from encoders on the robot as well as with results from previously published algorithms.

Key words: Direction Cosine Matrix, Euler Angles, Attitude Estimation, Kalman Filter.

1 INTRODUCTION

The attitude of an object is defined as the imaginary 3-D rotation that is needed to move the object from an initial reference orientation to its current orientation. Typically, the attitude is given relative to a frame of reference, usually specified by a Cartesian coordinate system. Accurate attitude information is essential in the controllers for many aerospace systems, such as satellites and unmanned aerial vehicles (UAVs). The rise of the smart phone and other wearable devices in recent years also requires attitude information for various applications, such as gesture recognition [1] [2] [3], video game controllers, rehabilitation [4], underwater robotic navigation [5] and assembly of parts [6]. Unfortunately, there exists no sensor that can directly measure attitude. Although the development of algorithms for attitude estimation is widely discussed in aerospace control literature, the sensors used for that purpose usually include multiple GPS receivers and other geological sensors, not just inertial sensors [7]. For robotic and daily life applications, GPS is often not usable. There exists a strong need to develop a systematic way to estimate the attitude of a rigid body using just an inexpensive inertial measurement unit (IMU), which includes accelerometers, gyroscopes and magnetometers.

A popular approach to attitude estimation is through integration of the angular rate measurements from a tri-axis gyroscope. The drifting effects due to gyroscope bias then need to be compensated by using additional measurement data from accelerometers and magnetometers. However, the formulation of the kinematic model with this approach and the corresponding estimator structure significantly vary in different papers. Since Euler angles are the most intuitive way to represent attitude information, several papers use them for some simple applications [2]. However, it is well known that Euler angles based estimation methods suffer from a singularity problem as the pitch angle approaches $\pm 90^\circ$ (gimbal lock phenomenon). Therefore, the applications of this method are limited to the cases

* Corresponding author: Rajesh Rajamani Tel. +1-612-626-7961. Fax +1-612-625-4344. This work was partially supported by the National Science Foundation under Grant CMMI 1562006.

Email addresses: wang1246@umn.edu (Yan Wang), rajamani@umn.edu (Rajesh Rajamani).

where the pitch motion is small. Another way to parametrize the attitude is the unit quaternion. In spite of complex quaternion algebra, it is the most popular way for attitude estimation in the navigation and aerospace societies [8]. Although the quaternion based approach solves the singularity problem, the inherent nonlinearity in the kinematic model for quaternions makes the estimator design quite challenging. The extended Kalman filter (EKF) or unscented Kalman filter (UKF) is a common tool used to perform nonlinear estimation [9] [10] [3] [11] with quaternions. One prominent drawback of the EKF and UKF is that global convergence cannot be guaranteed, which may lead to a divergence in case of large deviations between the initial condition of the estimator and the true system.

This paper proposes the estimation of the direction cosine matrix (DCM) instead of the Euler angles or quaternions. As will be shown in later sections, the DCM provides a more intuitive way to represent the attitude than quaternions and the singularity problem that paralyzes the Euler angles based approach also disappears. Although the DCM is a matrix with nine elements, only six of them are independent. The existing DCM estimation methods in the literature either require extra information from expensive sensors [12] or incorporate a nonlinear kinematic model and a nonlinear Kalman filter, such as EKF, UKF [13] [8] [14] [15] or nonlinear complementary filters [16]. This paper formulates the kinematics of the DCM as a linear time-varying state space model, which only necessitates a linear Kalman filter algorithm. Thus, global convergence can always be guaranteed and the nonlinearity in the model need not be considered. To further improve the robustness of the estimator with respect to the time-drifting bias in the tri-axis magnetometer, an automatic calibration method is developed. Finally, the estimation algorithm is demonstrated experimentally by using real measurement data collected from a 9-axis motion tracking sensors InvenSenses MPU9250. A comparison with the angular data measured from the encoders mounted on the joints of a 5-DOF robot is also presented. Compared with existing attitude methods reported in the literature, the primary contributions of this paper are listed below.

- (1) A direction cosine matrix (DCM) based attitude estimation method from the data of a 9-axis inertial measurement unit, which avoids singularities and nonlinear kinematic models, is proposed.
- (2) A novel algorithm to perform automatic calibration of the tri-axis magnetometer bias is developed.
- (3) An experimental verification of the attitude estimation results from an inexpensive smart phone grade inertial sensor using a 5-dof robot is presented.

The remainder of this paper is organized as follows. A brief review on Euler angles and their relationship with the DCM is presented in section 2. Section 3 discusses the development of the algorithm for the estimation of the DCM in detail. The automatic estimation of bias parameters in the tri-axis magnetometer is studied in section 4. The estimation results from the real experimental sensor data with a 5-DOF robotic arm are shown in section 5. Section 6 contains the final conclusions.

2 Kinematic Model for Attitude Estimation

There are three ways to parametrize the attitude of a rigid body, which are the Euler angles, direction cosine matrix (DCM) and quaternions [7] [17]. The DCM approach will be proposed in this paper. However, the Euler angles and DCM are strongly related from both intuition and a mathematical perspective. The definitions of these two representations together with their basic properties will be provided in the remainder of this section.

2.1 Euler Angles

The idea behind Euler rotations is to split the complete rotation of the coordinate system attached to an object into three simpler constitutive rotations, called precession, nutation, and intrinsic rotation, being each one of them an increment on one of the Euler angles. Therefore, any final orientation of an object in a 3-D space can be described using 3 rotation angles (Euler angles) in the specified orders [17] [18]. Suppose $(\bar{\mathbf{I}}, \bar{\mathbf{J}}, \bar{\mathbf{K}})$ and $(\bar{\mathbf{i}}, \bar{\mathbf{j}}, \bar{\mathbf{k}})$ represent the unit vectors of the inertial coordinate frame and a body-fixed frame respectively. The rotation order is assumed to be yaw(ψ)—pitch(θ)—roll(ϕ) as shown in Fig. 1 below, where $(\bar{\mathbf{i}}_{v1}, \bar{\mathbf{j}}_{v1}, \bar{\mathbf{k}}_{v1})$ and $(\bar{\mathbf{i}}_{v2}, \bar{\mathbf{j}}_{v2}, \bar{\mathbf{k}}_{v2})$ denote the unit vectors of the intermediate coordinates after yaw and pitch rotation. The final attitude of the body-fixed frame $(\bar{\mathbf{i}}, \bar{\mathbf{j}}, \bar{\mathbf{k}})$ is uniquely determined by the Euler angles ψ , θ and ϕ [7].

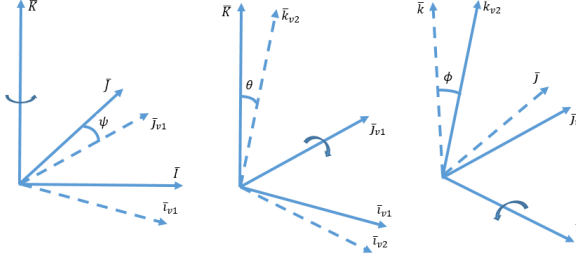


Fig. 1. Definition of Euler Angles

The rotation matrices corresponding to the three constitutive rotations are shown below [17] [19].

$$R_n^{v1} = \begin{bmatrix} c(\psi) & s(\psi) & 0 \\ -s(\psi) & c(\psi) & 0 \\ 0 & 0 & 1 \end{bmatrix}, \quad R_{v1}^{v2} = \begin{bmatrix} c(\theta) & 0 & -s(\theta) \\ 0 & 1 & 0 \\ s(\theta) & 0 & c(\theta) \end{bmatrix}, \quad R_{v2}^b = \begin{bmatrix} 1 & 0 & 0 \\ 0 & c(\phi) & s(\phi) \\ 0 & -s(\phi) & c(\phi) \end{bmatrix} \quad (1)$$

where $c(\cdot)$ and $s(\cdot)$ are the abbreviation of the $\cos(\cdot)$ and $\sin(\cdot)$ functions. The symbols n , $v1$, $v2$, b denote the inertial coordinate frame, the first and second intermediate coordinate frames and the body-fixed coordinate frame respectively. Based on the rotation matrices in (1), the coordinate transformation matrix from inertial coordinate frame to body-fixed frame is [18] [17]

$$\begin{bmatrix} \bar{\mathbf{i}} \\ \bar{\mathbf{j}} \\ \bar{\mathbf{k}} \end{bmatrix} = \underbrace{R_{v2}^b \cdot R_{v1}^{v2} \cdot R_n^{v1}}_{R_n^b} \begin{bmatrix} \bar{\mathbf{I}} \\ \bar{\mathbf{J}} \\ \bar{\mathbf{K}} \end{bmatrix} \quad (2)$$

where the coordinate transformation matrix R_n^b has the following form.

$$R_n^b = \begin{bmatrix} c(\psi)c(\theta) & c(\theta)s(\psi) & -s(\theta) \\ c(\psi)s(\phi)s(\theta) - c(\phi)s(\psi) & c(\phi)c(\psi) + s(\phi)s(\psi)s(\theta) & c(\theta)s(\phi) \\ s(\phi)s(\psi) + c(\phi)c(\psi)s(\theta) & c(\phi)s(\psi)s(\theta) - c(\psi)s(\phi) & c(\phi)c(\theta) \end{bmatrix} \quad (3)$$

It is clear from (3) that the Euler angles ψ , θ and ϕ uniquely determine the matrix R_n^b . However, this is not true the other way around as the pitch angle θ approaches $\pm 90^\circ$, which is referred as the singular problem in the literature [7].

2.2 Direction Cosine Matrix (DCM)

The rotation matrix R_n^b of (3) is also called the Direction Cosine Matrix (DCM) in the navigation literature [7]. Before the discussion of DCM, lets have a brief review of the definition of direction of cosines of a vector in a 3-D space.

As shown in Fig. 2, the direction cosines are defined as the cosines of the angles between the vector \mathbf{v} and the three unit basis vectors \mathbf{e}_x , \mathbf{e}_y and \mathbf{e}_z [7] [19].

$$\cos a = \frac{\mathbf{v} \cdot \mathbf{e}_x}{|\mathbf{v}|} = \frac{v_x}{\sqrt{v_x^2 + v_y^2 + v_z^2}}, \quad \cos b = \frac{\mathbf{v} \cdot \mathbf{e}_y}{|\mathbf{v}|} = \frac{v_y}{\sqrt{v_x^2 + v_y^2 + v_z^2}}, \quad \cos c = \frac{\mathbf{v} \cdot \mathbf{e}_z}{|\mathbf{v}|} = \frac{v_z}{\sqrt{v_x^2 + v_y^2 + v_z^2}} \quad (4)$$

From the above definition, an obvious property for the direction cosines is

$$\cos^2 a + \cos^2 b + \cos^2 c = 1 \quad (5)$$

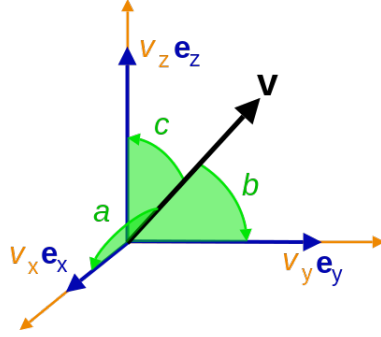


Fig. 2. Definition of Direction Cosine

If the vector \mathbf{v} is one of the unit basis vectors of another coordinate frame, the direction cosines in (4) constitute one of the column of the rotation matrix or DCM between the two coordinate frames. Therefore, each element of the DCM is indeed the cosine of the angle between the unit basis vectors of the two coordinate frames.

To facilitate the subsequent analysis of the attitude estimation, the DCM R_n^b is partitioned into the following form with three column vectors v_1 , v_2 and v_3 .

$$R_n^b = \begin{bmatrix} v_1 & v_2 & v_3 \end{bmatrix} \quad (6)$$

The orthonormality of R_n^b requires that v_1 , v_2 and v_3 satisfy the following constraints [7] [17]

$$v_1 \times v_2 = v_3, \quad v_2 \times v_3 = v_1, \quad v_3 \times v_1 = v_2 \quad (7)$$

and

$$\|v_i\| = 1, \quad \forall i = 1, 2, 3 \quad (8)$$

where the symbol \times denotes the cross product operator and $\|v_i\|$ represents the Euclidean norm of the vector v_i .

Remark 1. *The orthonormal conditions of the DCM R_n^b in (7) and (8) are equivalent to orthogonality of row and column vectors together with determinant constraint $\det(R_n^b) = 1$. Hence, the DCM R_n^b is ascribed to the SO(3) group in many literature, where SO stands for the phrase special orthogonal.*

2.3 Inertial Coordinate Frame

It has been shown that both Euler angles and DCM aim to quantify the attitude difference between the inertial coordinate frame and the body-fixed frame. For the body-fixed frame, there is no doubt that it is defined as the coordinate attached to the motion tracking sensor. For the inertial coordinate frame, its definition is quite flexible. However, a good choice of this reference coordinate may result in an estimation algorithm with less complexity.

In this paper, we propose to define the inertial coordinate frame, with unit vectors $\bar{\mathbf{I}}$, $\bar{\mathbf{J}}$ and $\bar{\mathbf{K}}$, according to the earth's magnetic field. It is shown in Fig. 3 below, that the unit vector $\bar{\mathbf{I}}$ is parallel to the horizontal plane and pointing to the magnetic north pole. The second unit vector $\bar{\mathbf{J}}$ is also in the horizontal plane but points to the west. The third one $\bar{\mathbf{K}}$ can be deduced by using the right-hand rule. As will be shown later, the advantage of this definition is that the magnetic field along the unit vector $\bar{\mathbf{J}}$ is zero which will simplify the DCM based estimation algorithm.

Remark 2. *It is well known that the geographic north pole and magnetic north pole do not coincide [20]. The difference between the two vectors pointing to the geographic and magnetic north pole respectively varies from location to location on the surface of the earth. The readers are referred to the latest navigation charts for accurate local information.*

3 Estimation of Direction Cosine Matrix (DCM)

Although the Euler angle is the most intuitive way to represent attitude information, it suffers from the singularity problem, which may cause the corresponding estimation algorithm to fail [7]. To overcome this dilemma, it is proposed to estimate the DCM R_n^b rather than the Euler angles.

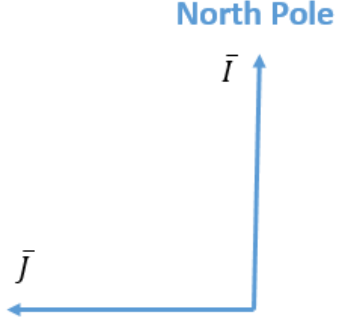


Fig. 3. Inertial Coordinate Frame

3.1 Measurement Model of DCM

In what follows, it will be shown that all the three column vectors v_1 , v_2 and v_3 defined in (6) can be computed from the accelerometer and magnetometer measurement signals a_x , a_y , a_z and b_x , b_y , b_z . Compared with the exiting methods reported in the literature, the algorithm presented in this paper does not need precise local earth magnetic field information, that is indispensable in solving the Wahbas problem [16] [7].

3.1.1 Estimation of the vector v_3

The gravitational acceleration in the inertial coordinate frame with A_x , A_y , A_z as the coordinates is

$$\begin{bmatrix} A_x \\ A_y \\ A_z \end{bmatrix} = \begin{bmatrix} 0 \\ 0 \\ -g \end{bmatrix} \quad (9)$$

where g is the gravitational acceleration constant. The vector v_3 can be directly obtained from the tri-axis acceleration measurements a_x , a_y and a_z as

$$v_3 = -\frac{1}{g} \begin{bmatrix} a_x \\ a_y \\ a_z \end{bmatrix} \quad (10)$$

To satisfy the normal condition in (8), the local gravitational acceleration constant g is chosen as $g = \sqrt{a_x^2 + a_y^2 + a_z^2}$.

3.1.2 Estimation of the vector v_1

Suppose B_x , B_y , B_z denote the coordinates of the earth magnetic field in the inertial coordinate frame defined in the last section. Hence, all the earth magnetic field is constrained in the plane spanned by B_X and B_Z . Hence, the magnitude of B_Y should be always 0. This leads to the coordinate transformation equation shown below.

$$\begin{bmatrix} B_x \\ 0 \\ B_Z \end{bmatrix} = \begin{bmatrix} v_1^T \\ v_2^T \\ v_3^T \end{bmatrix} \begin{bmatrix} b_x \\ b_y \\ b_z \end{bmatrix} \quad (11)$$

where b_x , b_y , and b_z are the measurement from tri-axis magnetometer. The vector v_3 is already available from the acceleration measurement in (10). Hence, the magnetic field component B_Z is directly computable as

$$B_Z = v_3^T \begin{bmatrix} b_x \\ b_y \\ b_z \end{bmatrix} \quad (12)$$

Moreover, the magnitude of the magnetic field in both inertial and body-fixed coordinates is equal.

$$b_x^2 + b_y^2 + b_z^2 = B_X^2 + B_Z^2 \quad (13)$$

Since B_X is defined as the component of the earth magnetic field that points to the North Pole, which is always positive, it implies

$$\begin{aligned} B_X &= \sqrt{(b_x^2 + b_y^2 + b_z^2) - B_Z^2} \\ &= \sqrt{(b_x^2 + b_y^2 + b_z^2) - \left[\frac{1}{g}(a_x b_x + a_y b_y + a_z b_z) \right]^2} \end{aligned} \quad (14)$$

Then, the vector v_1 can be calculated as

$$\begin{aligned} v_1 &= \frac{1}{B_X} \left(\begin{bmatrix} b_x \\ b_y \\ b_z \end{bmatrix} - B_Z v_3 \right)_1 \\ &= \frac{\sqrt{(b_x^2 + b_y^2 + b_z^2) - \left[\frac{1}{g}(a_x b_x + a_y b_y + a_z b_z) \right]^2}}{\begin{bmatrix} b_x \\ b_y \\ b_z \end{bmatrix} - \left[\frac{1}{g^2}(a_x b_x + a_y b_y + a_z b_z) \right] \begin{bmatrix} a_x \\ a_y \\ a_z \end{bmatrix}} \end{aligned} \quad (15)$$

3.1.3 Estimation of the vector v_2

Finally, the vector v_2 can be derived from v_1 and v_3 together with the following kinematic constraint.

$$v_2 = v_3 \times v_1 \quad (16)$$

where the symbol \times denotes the cross product operator.

Remark 3. As can be seen from the algebraic model in (15), (16) and (10), it is only possible to obtain the estimation of the whole DCM R_n^b with both accelerometer and magnetometer data. If the acceleration data is just available, only the third column v_3 can be estimated. With the assistance of the magnetometer data, the first column v_1 , together with second column v_2 , can also be estimated.

Remark 4. The above procedure to compute the column vectors of v_1 , v_2 and v_3 is valid everywhere on the surface of the earth, except the area close to the magnetic north pole where the magnetic field component B_X approaches 0.

3.2 Orthonormal Condition

The kinematic equations to derive the three column vectors v_1 , v_2 and v_3 in the DCM R_n^b from the accelerometer and magnetometer measurement are shown in (15), (16) and (10) respectively. The question is whether they satisfy the necessary orthonormal condition in (7) and (8). The answer is yes, which is proved by the following theorem.

Theorem 1. The three column vectors v_1 , v_2 and v_3 in (15), (16) and (10) constitute three orthonormal basis vectors in the 3-D Euclidean space.

Proof. The normal condition of the vector v_3 in (10) has already been proved by choosing the local gravitational acceleration constant g as $g = \sqrt{a_x^2 + a_y^2 + a_z^2}$. For the vector v_1 , the equations shown below can be derived from

(12) (13) and (15).

$$\begin{aligned}\|v_1\|^2 &= \frac{1}{B_X^2} \left(\left\| \begin{bmatrix} b_x \\ b_y \\ b_z \end{bmatrix} \right\|^2 - 2B_Z v_3^T \begin{bmatrix} b_x \\ b_y \\ b_z \end{bmatrix} + B_Z^2 \right) \\ &= \frac{1}{B_X^2} \left(\left\| \begin{bmatrix} b_x \\ b_y \\ b_z \end{bmatrix} \right\|^2 - B_Z^2 \right) = 1\end{aligned}\tag{17}$$

and

$$\langle v_1, v_3 \rangle = \frac{1}{B_X} \left(v_3^T \begin{bmatrix} b_x \\ b_y \\ b_z \end{bmatrix} - B_Z \right) = 0\tag{18}$$

Therefore, it can be concluded that the vectors v_1 and v_3 constitute an orthonormal pair. Because the third one v_2 is the cross product of v_1 and v_3 according to (16), it completes the orthonormal basis in the 3-D Euclidean space. \square

3.3 Probability Distribution Functions (PDFs) of v_1 , v_2 and v_3

Beyond the orthonormal property, another question worth to study is whether the three column vectors v_1 , v_2 and v_3 computed from the measurement signals a_x , a_y , a_z and b_x , b_y , b_z with additive zero-mean Gaussian distributed noise also follow the unbiased Gaussian distribution. As can be seen from (15), (16) and (10) that all the three vectors are related to the measurement signals in a very complex way, which makes the prediction of the probability distribution functions (PDFs) of the vectors v_1 , v_2 and v_3 quite challenging. However, it will be proved that these vectors are approximately unbiased Gaussian distributed if the noise contained in the measurement signals follows Gaussian distribution with zero mean and sufficiently small variance.

Theorem 2. *If each of the signals a_x , a_y , a_z and b_x , b_y , b_z collected from the tri-axis accelerometer and magnetometer contains a Gaussian distributed measurement noise with zero mean and small enough variance, the resulting column vectors v_1 , v_2 and v_3 computed from (15), (16) and (10) also follow the unbiased Gaussian distribution.*

Proof. Let the symbol y denote the collection of the six measurement signals a_x , a_y , a_z and b_x , b_y , b_z as

$$y = [a_x \ a_y \ a_z \ b_x \ b_y \ b_z]^T\tag{19}$$

and ϵ represents the corresponding measurement noise which is a multivariate Gaussian distributed random variable $\epsilon \sim N(0, P)$. If all the elements in the covariance matrix P are sufficiently small, any differentiable function $f(y)$ can be approximated by the 1st-order Taylor approximation.

$$f(y) = f(y_n + \epsilon) \approx f(y_n) + \left[\frac{\partial f}{\partial y} \right]_{y=y_n} \epsilon\tag{20}$$

where y_n is the deterministic noise-free signal and $[\partial f / \partial y]$ is the Jacobian matrix. Obviously, the zero-mean property of ϵ leads to

$$E[f(y)] \approx E[f(y_n)]\tag{21}$$

Furthermore, the affine dependence of $f(y)$ on $\epsilon \sim N(0, P)$ implies that the function $f(y)$ also follows the unbiased Gaussian distribution [21] [22].

Since each function in (15), (16) and (10) is 1st-order differentiable, v_1 , v_2 and v_3 can be approximated in the form of (20). Therefore, it can be concluded that v_1 , v_2 and v_3 follow the unbiased Gaussian distribution. \square

Remark 5. *The covariance matrix R_i of the vector v_i , $i = 1, 2, 3$ can also be obtained from the 1st-order Taylor approximation in (20)*

$$R_i = \left[\frac{\partial f_i}{\partial y} \right]_{y=y_n} P \left[\frac{\partial f_i}{\partial y} \right]_{y=y_n}^T\tag{22}$$

where $P = E(\epsilon\epsilon^T)$ is assumed to be a diagonal matrix and $f_i(\cdot)$ denotes one of the nonlinear functions in (15), (16) and (10).

3.4 Kalman Filter for Attitude Estimation

Although the algebraic relationship between the three column vectors v_1 , v_2 and v_3 in the DCM R_n^b and the acceleration and magnetic field measurement is revealed in (15) (16) and (10), those estimates are static estimation and will have dynamic error. The Kalman filter algorithm that fuses the dynamic data from the tri-axis gyroscope and the static data from (15) (16) and (10), is applied to obtain the optimal smoothed attitude estimation in this paper.

3.4.1 Kinematic model for Time Update

The kinematic model of the DCM R_n^b used in the prediction step of the Kalman filter algorithm is the integrator of the angular rate measurement from the tri-axis gyroscope as shown in (23) [7]

$$\dot{R}_n^b = S(\omega)R_n^b \quad (23)$$

where $\omega = [\omega_x \ \omega_y \ \omega_z]$ are the measurements from a tri-axis gyro, which are treated as the time-varying parameters in the model. $S(\omega)$ is a skew-symmetric matrix.

$$S(\omega) = \begin{bmatrix} 0 & \omega_z & -\omega_y \\ -\omega_z & 0 & \omega_x \\ \omega_y & -\omega_x & 0 \end{bmatrix} \quad (24)$$

To implement the state estimation algorithm, such as Luenberger observer or Kalman filter, in the microprocessor powered embedded system, the kinematic differential equation in (23) needs to be discretized. However, such an accurate discretization is not a trivial procedure since the orthonormal property in (7) and (8) will not be automatically guaranteed by those commonly used approaches, such as 1st-order Euler differentiation. In what follows, a discrete-time model that rigorously guarantees the orthonormal property will be presented.

At first, we assume that the tri-axis angular rate ω keeps constant during each sampling interval. Then, the DCM at two neighboring sampling points indexed by k and $k + 1$ are related by

$$R_n^b[k + 1] = e^{S(\omega)h} R_n^b[k] \quad (25)$$

where h is the sampling time. In the remainder of this paper, (25) will be used as the discrete-time version of the kinematic model in (23). Lemma 1 shows that the orthonormal property is preserved by the discrete-time update equation in (25).

Lemma 1. *The DCM $R_n^b[k + 1]$ in (25) satisfies the orthonormal property as shown in (7) and (8) if $R_n^b[k]$ also holds this property.*

Proof. Since $S(\omega)$ in (24) is a skew-symmetric matrix, the matrix exponential $e^{S(\omega)h}$ is an orthogonal matrix with determinant 1. This implies that $R_n^b[k + 1]$ in (25) is also an orthogonal matrix. Its determinant can be computed as

$$\begin{aligned} \det(R_n^b[k + 1]) &= \det(e^{S(\omega)h}) \cdot \det(R_n^b[k]) \\ &= \det(R_n^b[k]) = 1 \end{aligned} \quad (26)$$

Hence, $R_n^b[k + 1]$ also belongs to $SO(3)$ group. \square

The next question is how to accurately compute the matrix exponential $e^{S(\omega)h}$. Although there is a thorough discussion about this issue using the eigenvalue decomposition approach in the linear systems and control textbooks [23], those computational expensive approaches are prohibitive for implementation in the real-time system with very limited computational resources. On the other hand, finite order truncation of the Taylor series in (27) is widely used in the embedded computing platform. It is also obvious that the 1st-order Euler differentiation is just the 1st-order truncation of this infinite series.

$$e^{S(\omega)h} = \sum_{n=0}^{\infty} \frac{h^n}{n!} S^n(\omega) \quad (27)$$

Beyond the finite-order approximation, it will be presented that the mathematical property of the skew symmetric matrix allows to exactly compute the matrix exponential $e^{S(\omega)h}$.

Lemma 2. *The matrix exponential $e^{S(\omega)h}$ can be exactly computed as the matrix trigonometry function shown in (28)*

$$e^{S(\omega)h} = I + \sin(h\|\omega\|)S_n(\omega) + (1 - \cos(h\|\omega\|))S_n^2(\omega) \quad (28)$$

where I denotes a 3×3 identity matrix and $\|\omega\| = \sqrt{\omega_x^2 + \omega_y^2 + \omega_z^2}$. $S_n(\omega)$ is the normalized skew symmetric matrix $S(\omega)$ shown as

$$S_n(\omega) = \begin{bmatrix} 0 & \frac{\omega_z}{\|\omega\|} & -\frac{\omega_y}{\|\omega\|} \\ -\frac{\omega_z}{\|\omega\|} & 0 & \frac{\omega_x}{\|\omega\|} \\ \frac{\omega_y}{\|\omega\|} & -\frac{\omega_x}{\|\omega\|} & 0 \end{bmatrix} \quad (29)$$

Proof. The proof of (28) can be seen in [24] \square

As shown in (28), the matrix exponential $e^{S(\omega)h}$ is a state transition matrix with time-varying parameters ω for the discrete-time state space model. For the linear time-varying system with zero-mean Gaussian distributed measurement noise as proved in Theorem 2, the Kalman filter is a perfect tool to perform the state estimation [22] [25]. To apply the state estimation algorithm, such as Luenberger observer or Kalman filter, the kinematic differential equation in (23) needs to be transformed into the standard state space model shown below.

$$x_{k+1} = A(\omega_k)x_k, \quad y_k = Cx_k \quad (30)$$

where the subscript k denotes the index of the sampling time. The state matrix $A(\omega_k)$ is a linear matrix function of the time-varying parameters ω_k as shown in (33). According to the partition of R_n^b in (6), the differential equation for the column vector v_i is

$$v_i[k+1] = e^{S(\omega_k)h}v_i[k], \quad i = 1, 2, 3 \quad (31)$$

Since all the three vectors v_1 , v_2 and v_3 need to be estimated, they can be lumped together in the state vector x_k as

$$x_k = \begin{bmatrix} v_1^T[k] & v_2^T[k] & v_3^T[k] \end{bmatrix}^T \quad (32)$$

Then, the corresponding state matrix $A(\omega_k)$ and the output matrix C in (30) have the following form

$$A(\omega_k) = \begin{bmatrix} e^{S(\omega_k)h} & 0_3 & 0_3 \\ 0_3 & e^{S(\omega_k)h} & 0_3 \\ 0_3 & 0_3 & e^{S(\omega_k)h} \end{bmatrix}, \quad C = I_9 \quad (33)$$

where 0_3 and I_9 are the 3×3 zero and 9×9 identity matrices respectively. To achieve the optimal performance, the covariance matrices of the process disturbance and measurement noise should be properly selected. For the measurement noise, the covariance matrix R_i of the individual vector v_i , $i = 1, 2, 3$ in the DCM has already been shown in (22). Instead of the noise free value y_n , the Jacobian matrix can be evaluated at the measured value $y = y_n + \epsilon$ to make (22) practically implementable in the Kalman filter. For the process disturbance, which results from the noise contained in the angular rate measurement from the tri-axis gyro, the discrete-time state equation in (30) can be reformulated as

$$\begin{aligned} x_{k+1} &= A(\omega_{k,n})x_k = A(\omega_{k,m} + \epsilon_\omega)x_k \\ &\approx A(\omega_{k,m})x_k + \left[\frac{\partial A(\omega)x_k}{\partial \omega} \right]_{\omega=\omega_{k,m}} \epsilon_\omega \end{aligned} \quad (34)$$

where $\omega_{k,n}$, $\omega_{k,m}$ and ϵ_ω are the nominal (noise-free), measured angular rate and the gyroscopic noise at k th sampling time respectively. Similar to Theorem 2, it can be concluded that the 1st-order Taylor approximation in (34) leads to an unbiased process disturbance if the gyroscopic noise $\epsilon_\omega \sim N(0, P_\omega)$ with small enough amplitude of the elements in the covariance matrix P_ω . Accordingly, the covariance matrix Q of the process disturbance can be obtained as

$$Q = \left[\frac{\partial A(\omega)x_k}{\partial \omega} \right]_{\omega=\omega_{k,m}} \cdot P_\omega \cdot \left[\frac{\partial A(\omega)x_k}{\partial \omega} \right]_{\omega=\omega_{k,m}}^T \quad (35)$$

With the available covariance matrices in (35) and (22), the readers are referred to [26] [22] for the standard linear discrete-time Kalman filter equations, which are ignored here.

3.4.2 $SO(3)$ -Constrained Kalman Filter Algorithm

With (25) as the kinematic process model and the measurement model in (15), (16) and (10), it seems that the Kalman filter algorithm is directly applicable to obtain the optimal unbiased attitude estimation. However, the orthonormal constraint in (7) and (8) is not automatically satisfied by the traditional unconstrained Kalman filter algorithm. To guarantee the estimation result belongs to the $SO(3)$ group, the Kalman filter algorithm should be augmented to incorporate the orthonormal constraint [27]. At k th instant, the $SO(3)$ -constrained Kalman filter algorithm is summarized below.

$SO(3)$ -Constrained Kalman Filter Algorithm for DCM Estimation

Prediction Step : $\hat{x}_k^- = A(\omega_k)\hat{x}_{k-1}$
 $P_k^- = A(\omega_k)P_{k-1}^+A(\omega_k)^T + Q_{k-1}$

Kalman Gain : $K_k = P_k^- C^T (CP_k^- C^T + R_k)^{-1}$

Measurement Update : $\hat{x}_k^+ = \hat{x}_k^- + K_k(y_k - C\hat{x}_k^-)$
 $P_k^+ = (I - K_k C)P_k^-$

$SO(3)$ Projection : Solving the following $SO(3)$ constrained minimization problem

$$\hat{x}_k = \arg \min_{\hat{x}_k \in SO(3)} \text{trace}[(\hat{x}_k - \hat{x}_k^+)^T (\hat{x}_k - \hat{x}_k^+)]$$

ω_k is the tri-axis gyroscope data and y_k is the measurement of the DCM state from (15), (16) and (10). \hat{x}_k denotes the estimation of the state in (32) that satisfies the $SO(3)$ constraint.

The $SO(3)$ projection problem in the last step of the above algorithm is equivalent to the Wahbas problem [7] shown in (36), for which there exists various standard analytical solutions.

$$\underset{R \in SO(3)}{\text{minimize}} \frac{1}{2} \text{trace}[(R - R_{unc})^T (R - R_{unc})] \quad (36)$$

The matrix R_{unc} is constructed by the unconstrained estimation \hat{x}_k^+ from the measurement update step. Suppose R_{unc} has the following singular value decomposition (SVD)

$$R_{unc} = V\Sigma U^T \quad (37)$$

Then, the solution of the $SO(3)$ Projection Problem R is

$$R = V \text{diag}[I_2, \det V \det U] U^T \quad (38)$$

The readers are referred to [7] for detailed derivation procedure.

4 Estimation of the Bias of the Tri-Axis Magnetometer

Both the accelerometer and magnetometer measurement data always contain bias errors in real-world applications. Hence, it is important to get an accurate estimate of the bias before the application of the motion tracking sensor.

Since the gravitational acceleration g is insensitive to the environment and roughly keeps constant along the earth's surface, the offset variables in the accelerometer can be calibrated with rather good accuracy before real applications.

Hence, only small bias errors will remain in the accelerometer data after the calibration. On the other hand, the offset variables in the magnetometer may have a large variation due to the influence of unknown local external magnetic field source and due to offsets from the magnetic material inside the magnetometer. It will be shown that the bias in the tri-axis magnetometer can be estimated from the tri-axis accelerometer data without requiring any the external reference sensors in the remainder of this section. By performing a simple calibration procedure, the bias in the magnetometer can be highly reduced.

Considering the bias in the earth magnetic field measurement, the equations related to the estimation of the bias are shown below

$$B_Z = v_3^T \begin{bmatrix} b_x \\ b_y \\ b_z \end{bmatrix} \text{ and } \begin{bmatrix} \bar{b}_x \\ \bar{b}_y \\ \bar{b}_z \end{bmatrix} = \begin{bmatrix} b_x \\ b_y \\ b_z \end{bmatrix} + \begin{bmatrix} \Delta b_x \\ \Delta b_y \\ \Delta b_z \end{bmatrix} \quad (39)$$

where b_x, b_y, b_z are the true earth magnetic field in the body-fixed coordinate. $\bar{b}_x, \bar{b}_y, \bar{b}_z$ are the measured earth magnetic field in the body-fixed coordinate. $\Delta b_x, \Delta b_y, \Delta b_z$ are the bias along the tri-axis of the magnetometer. B_Z is the component of the earth magnetic field perpendicular to the earth surface in the inertial coordinate frame. v_3 is the third column vector of the DCM R_n^b in (6). To clarify the estimation goals, both known and unknown variables in (39) are summarized in what follows.

- Known Variables: $\bar{b}_x, \bar{b}_y, \bar{b}_z$ and v_3
- Unknown Variables: $b_x, b_y, b_z, \Delta b_x, \Delta b_y, \Delta b_z$ and B_Z

Since there are more unknown variables than the equations for a single set of data, it implies that more sets of data are necessary for bias estimation. The bias estimation method presented in this section is based on the following assumption.

Assumption 1. *The offset variables $\Delta b_x, \Delta b_y, \Delta b_z$ and the vertical component of the earth magnetic field B_Z in the inertial coordinate are constants in all the calibration data sets.*

This assumption implies that there are 7 unknown variables and 4 equations in each calibration experiment. Among the 7 unknown variables, 4 of them keep unchanged in all the experiments. Therefore, only 3 new unknown variables, but 4 new equations are added in each experiment. Then, Lemma 3 answers the question how many sets of data are needed to estimate all the unknown offset variables.

Lemma 3. *At least 4 sets of measurement data are needed to estimate all the unknown but constant offset variables $\Delta b_x, \Delta b_y$ and Δb_z .*

Proof. Suppose n sets experimental data are available. Then, $7 + 3(n - 1)$ unknown variables and $4n$ equations can be obtained. Therefore, the minimum value of n , such that $7 + 3(n - 1) \leq 4n$, is 4. \square

In this section, the discussion will only focus on the case with 4 sets of calibration data. For each set of data, the measurement equation can be written as $y_{m,i} = H_i x_i$ where i denotes the index of the data set. The measurement vector $y_{m,i}$ and the unknown parameter vector x_i are

$$\begin{aligned} y_{m,i} &= \left[0 \ \bar{b}_{x,i} \ \bar{b}_{y,i} \ \bar{b}_{z,i} \right]^T \\ x_i &= \left[B_Z \ \Delta b_x \ \Delta b_y \ \Delta b_z \ b_{x,i} \ b_{y,i} \ b_{z,i} \right]^T \end{aligned} \quad (40)$$

The linear mapping matrix H_i from the i th set of data is

$$H_i = \begin{bmatrix} 1 & 0_{1 \times 3} & -v_{3,i}^T \\ 0_{3 \times 1} & I_3 & I_3 \end{bmatrix} \quad (41)$$

where $0_{1 \times 3}$ and $0_{3 \times 1}$ denote a 1×3 zero matrix and its transpose respectively. I_3 is a 3×3 identity matrix.

If 4 sets of calibration data are available, all the measurement equations can be lumped together as

$$Y_m = H X \quad (42)$$

where the measurement vector Y_m and unknown parameter vector X are

$$\begin{aligned} Y_m &= \left[y_{1,m}^T \ y_{2,m}^T \ y_{3,m}^T \ y_{4,m}^T \right]^T \\ X &= \left[x_1^T \ x_2^T \ x_3^T \ x_4^T \right]^T \end{aligned} \quad (43)$$

The corresponding linear mapping matrix H becomes

$$H = \begin{bmatrix} 1 & 0_{1 \times 3} & -v_{3,1}^T & 0_{1 \times 3} & 0_{1 \times 3} & 0_{1 \times 3} \\ 0_{3 \times 1} & I_3 & I_3 & 0_3 & 0_3 & 0_3 \\ 1 & 0_{1 \times 3} & 0_{1 \times 3} & -v_{3,2}^T & 0_{1 \times 3} & 0_{1 \times 3} \\ 0_{3 \times 1} & I_3 & 0_3 & I_3 & 0_3 & 0_3 \\ 1 & 0_{1 \times 3} & 0_{1 \times 3} & 0_{1 \times 3} & -v_{3,3}^T & 0_{1 \times 3} \\ 0_{3 \times 1} & I_3 & 0_3 & 0_3 & I_3 & 0_3 \\ 1 & 0_{1 \times 3} & 0_{1 \times 3} & 0_{1 \times 3} & 0_{1 \times 3} & -v_{3,4}^T \\ 0_{3 \times 1} & I_3 & 0_3 & 0_3 & 0_3 & I_3 \end{bmatrix} \quad (44)$$

where $H \in R^{16 \times 16}$. The question is in what condition the matrix H dose not lose rank such that the unknown parameter vector X in (42) can be estimated uniquely.

Theorem 3. *The matrix H in (44) is full rank if and only if the following 3×3 real matrix is nonsingular.*

$$\begin{bmatrix} v_{3,2}^T - v_{3,1}^T \\ v_{3,3}^T - v_{3,1}^T \\ v_{3,4}^T - v_{3,1}^T \end{bmatrix} \quad (45)$$

Proof. If: The matrix H in (44) is transformed into the matrix shown in (46) after a series of elementary row operations.

$$H \sim H_1 = \begin{bmatrix} 1 & v_{3,1}^T & 0_{1 \times 3} & 0_{1 \times 3} & 0_{1 \times 3} & 0_{1 \times 3} \\ 0_{3 \times 1} & I_3 & I_3 & 0_3 & 0_3 & 0_3 \\ 1 & v_{3,2}^T & 0_{1 \times 3} & 0_{1 \times 3} & 0_{1 \times 3} & 0_{1 \times 3} \\ 0_{3 \times 1} & I_3 & 0_3 & I_3 & 0_3 & 0_3 \\ 1 & v_{3,3}^T & 0_{1 \times 3} & 0_{1 \times 3} & 0_{1 \times 3} & 0_{1 \times 3} \\ 0_{3 \times 1} & I_3 & 0_3 & 0_3 & I_3 & 0_3 \\ 1 & v_{3,4}^T & 0_{1 \times 3} & 0_{1 \times 3} & 0_{1 \times 3} & 0_{1 \times 3} \\ 0_{3 \times 1} & I_3 & 0_3 & 0_3 & 0_3 & I_3 \end{bmatrix} \quad (46)$$

The following observations can be obtained from the the matrix H_1 in (46):

- (1) The row 2, 3, 4, row 6, 7, 8, row 10, 11, 12 and row 14, 15, 16 are all linearly independent.
- (2) Any vector in the row 1, 5, 9 and 13 are linearly independent with the row 2, 3, 4, row 6, 7, 8, row 10, 11, 12 and row 14, 15, 16.

For further rank analysis, the following matrix G composed of the vectors in the row 1, 5, 9 and 13 of the matrix

H_1 is shown as

$$G = \begin{bmatrix} 1 & v_{3,1}^T & 0_{1 \times 12} \\ 1 & v_{3,2}^T & 0_{1 \times 12} \\ 1 & v_{3,3}^T & 0_{1 \times 12} \\ 1 & v_{3,4}^T & 0_{1 \times 12} \end{bmatrix} \sim \begin{bmatrix} 1 & v_{3,1}^T & 0_{1 \times 12} \\ 0 & v_{3,2}^T - v_{3,1}^T & 0_{1 \times 12} \\ 0 & v_{3,3}^T - v_{3,1}^T & 0_{1 \times 12} \\ 0 & v_{3,4}^T - v_{3,1}^T & 0_{1 \times 12} \end{bmatrix} \quad (47)$$

where $0_{1 \times 12}$ denotes a 1×12 zero matrix and the symbol \sim represents the elementary row operation, which does not change the rank of the matrix [28]. Obviously, the nonsingular property of the matrix in (45) implies that none of the rows of the matrix in (47) can be transformed into a zero row vector through elementary operations. Hence, it is guaranteed that the matrix G in (47) is full row rank. Since all the rows of the matrix H_1 in (46) are linearly independent, it can be concluded that the matrix H in (44) is full rank.

Only if: Suppose the matrix in (45) is singular. Then, the matrix G in (47) will lose rank, which implies the rank deficiency of the matrices H_1 and H . Therefore, the matrix in (45) cannot be singular, if the matrix H in (44) is full rank. \square

Remark 6. An obvious fact from Theorem 3 is that the matrix H in (44) will lose rank if there exist two sets of data with indices i, j , $i \neq j$ such that $v_{3,i} = v_{3,j}$.

An implication from Theorem 3 is that whether the unknown but constant offset variables Δb_x , Δb_y and Δb_z can be estimated from 4 sets of measurement data only depends on the vectors $v_{3,i}^T$, $i = 1, 2, 3, 4$. According to the partition of the DCM in (3), the vector $v_{3,i}^T$ for the i th set of data is

$$v_{3,i}^T = \left[-\sin \theta_i \cos \theta_i \sin \phi_i \cos \phi_i \cos \theta_i \right] \quad (48)$$

where θ_i , ϕ_i are the pitch and roll angles contained in the i th set of calibration data. Once four sets of pitch and roll angles that guarantee the nonsingularity of the matrix H in (44) is found, the unknown vector X including the offset variables can be estimated as

$$X = H^{-1}Y_m \quad (49)$$

Remark 7. Although the bias estimation only focuses on the case in which the data sets are collected from 4 calibration experiments with different pitch and roll angles, the result can be extended to more than 4 sets of data. If the linear mapping matrix H in (42) does not suffer from the rank deficiency, the estimation of the unknown vector X can be obtained from the linear least square estimator as

$$X = (H^T H)^{-1} H^T Y_m \quad (50)$$

Remark 8. The automatic bias calibration algorithm discussed above only assumes that the offset parameters of the tri-axis magnetometer keep as constants during the data collection. This algorithm can be implemented periodically to continuously estimate the time-varying offset parameters without any effort from the user.

5 Experimental Results

To validate the DCM based attitude estimation algorithm presented in this paper, a 9-axis motion tracking sensor, the InvenSenses MPU9250, is used for demonstration. A photograph of the PCB for MPU9250 can be seen in Fig. 4. The sensor board contains a tri-axis accelerometer, a tri-axis gyroscope and a tri-axis magnetometer (9 sensor signals in total). The experimental data shows that the variance and maximum measurement error for the accelerometer are $0.012g$ and $\pm 0.02g$ respectively under normal operation condition. For the magnetometer, the variance and maximum measurement error are $43\mu T$ and $\pm 65\mu T$.

Since it is hard to directly measure the Euler angles (or other attitude information) of a single PCB during 3D motion, the 9-axis motion sensor must be attached to a device with a sensing capability to measure the actual or true attitude information. The validation experimental platform used in this section is a 5-DOF robot as shown in Fig. 5. The 9-axis motion sensor is attached on the end-effector of the 5-DOF robot such that the attitude of the last link can be estimated from the 9-axis data by applying the algorithm in the previous sections. Furthermore, each joint of the robot is installed with an encoder to measure the relative angle between two connected links. Therefore, the attitude of each link can be read out from all the encoder data, which will be treated as a reference for the estimation algorithm. Various trajectories of the robotic arm are executed in the experiments.



Fig. 4. The PCB for MPU9250

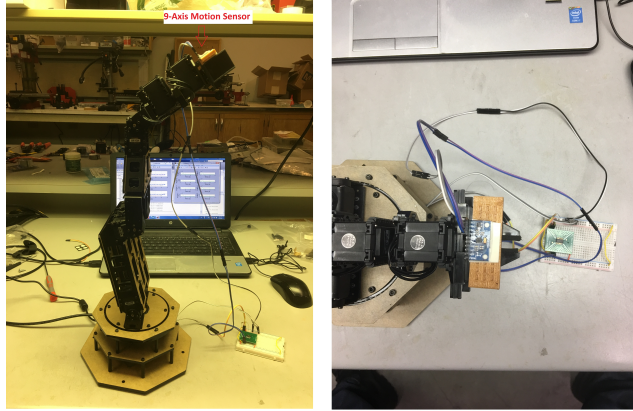


Fig. 5. The 5-DOF Robotic Arm and the 9-Axis Motion Sensor

5.1 Kinematic Analysis of the 5-DOF Robotic Arm

The diagram for the kinematic analysis of the 5-DOF robotic arm together with the definition of the body-fixed coordinates attached to each link labeled from 1 to 5 can be seen in Fig. 6. Each link is allowed to rotate around only one axis in the body-fixed coordinate. The classification of the links according to their rotation axes is show as

$$\text{x-axis: } 1, \quad \text{y-axis: } 2, 3, 4, \quad \text{z-axis: } 5$$

Since the robot in Fig. 6 consists of a chain of 5 links connected in series, the DCM of the end link can be obtained as the product of all the individual DCM

$$R_n^5 = R_4^5(\theta_5) \cdot R_3^4(\theta_4) \cdot R_2^3(\theta_3) \cdot R_1^2(\theta_2) \cdot R_n^1(\theta_1) \quad (51)$$

where θ_i , $i = 1, \dots, 5$ denotes the relative angle between connected links that can be measured by the encoder attached on the corresponding joint. (51) is also called the forward kinematics equation of the serial chain in the robotics literature [17] [29].

5.2 Experimental Data Processing

In the validation experiments, the sampling frequency for the motion sensor and encoders is 50Hz. The 5-DOF robot will be excited by different trajectories to verify whether the estimated DCM of the end link from the 9-axis motion sensor data matches the one shown in (51) from the encoder data. However, the mechanical configuration of the robotic arm together with the encoders may not (or is prohibitive to) coincide with the inertial coordinate defined in section 2. For example, the DCM estimation algorithm presented above uses the vector pointing to the magnetic north pole as a reference for zero yaw angle, which may significantly differ from the zero of the angle θ_1 . Another example is the encoder of link 2 in Fig. 6 may not show 0 or 180 degree of pitch angle when the link 2 is parallel to the horizontal surface. To make the DCM computed from the encoders data comparable to the estimation from the motion sensor, it is necessary to calibrate the offset of all the encoders, which is the difference between the zero of the encoders data and the zero of the Euler angles, before the validation experiments. The following protocol provides more details about the data processing procedure for the calibration of the zero angles of the encoders data.

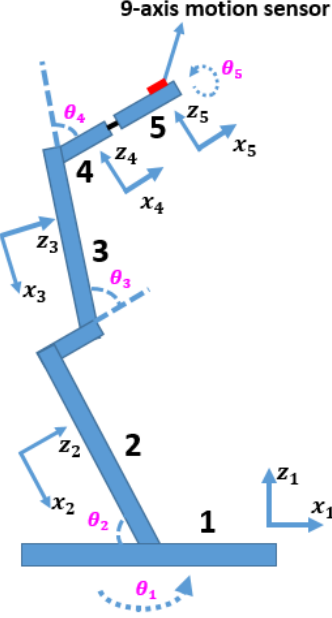


Fig. 6. Diagram of 5-DOF Robotic Arm and body-fixed coordinates

5.2.1 Mapping from encoders data to Euler angles

According to the rotation axis of each link, the mapping from the encoders data to Euler angles of the end-effector is shown as

$$\text{Yaw: } \theta_1, \quad \text{Pitch: } \theta_2 + \theta_3 + \theta_4, \quad \text{Roll: } \theta_5$$

5.2.2 Mechanical configuration and data collection

First, the body-fixed x axis of link 3, 4 and 5 are set to the same direction as that of link 2, which implies that all these links share the same pitch angle with link 2. Then, the 5-DOF robotic arm is configured at different static position to collect the data for offset estimation.

5.2.3 Estimation of the offset

Once the data of the 9-axis motion sensor is collected at different position, the DCM together with the Euler angles can be estimated from the algorithm presented in the previous sections. By comparing with the encoders data, the estimation of the offset of θ_1 , θ_2 and θ_5 can be obtained. For example, the offset $\theta_{1,0}$ of θ_1 can be estimated by solving the following linear least square problem

$$\hat{\theta}_{1,0} = \arg \min \sum_{i=1}^n \left(\theta_1^{(i)} - \theta_{1,0} - \psi_e^{(i)} \right)^2 \quad (52)$$

where n is the total number of position. $\theta_1^{(i)}$ and $\psi_e^{(i)}$ are the encoder data for θ_1 and the estimation of the yaw angle at the i th position respectively. The solution of (52) is shown as

$$\hat{\theta}_{1,0} = \frac{1}{n} \sum_{i=1}^n \left(\theta_1^{(i)} - \psi_e^{(i)} \right) \quad (53)$$

The offset of θ_2 and θ_5 can be obtained in a similar way by comparing the estimated pitch and roll angles with the corresponding encoders data. For θ_3 and θ_4 , the encoders data directly shows the offset because of the zero relative angle among link 2, 3 and 4. For example, the estimation of the offset $\theta_{3,0}$ of θ_3 can be obtained by taking the

average of the encoder measurement at all position.

$$\hat{\theta}_{3,0} = \frac{1}{n} \sum_{i=1}^n \theta_3^{(i)} \quad (54)$$

After getting the offset estimation of all the encoders, the forward kinematic chain in (51) can be applied to compute the DCM reference for validation experiments.

5.3 Estimation Results

The DCM estimation results of three validation experiments will be reviewed in what follows. The 5-DOF robotic arm is made to follow different trajectories in each experiment.

5.3.1 1st Validation Experiment

The robot end-effector follows a periodic oscillatory motion of yaw and pitch angles around its initial position.

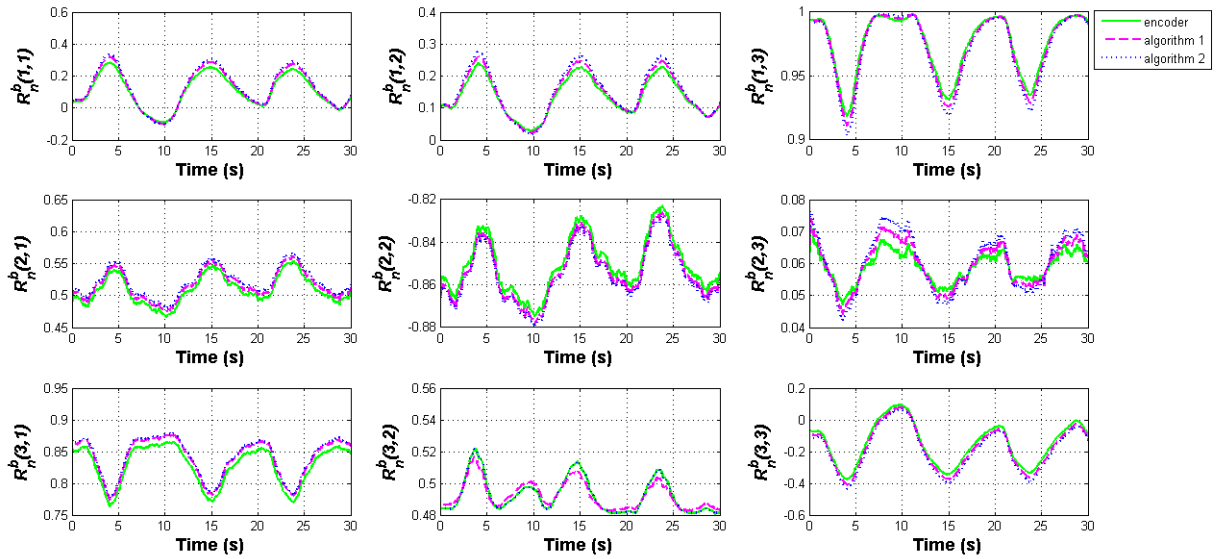


Fig. 7. The DCM estimation results in the first experiment

5.3.2 2nd Validation Experiment

The robot end-effector mimics the movement of hand waving of a human arm.

5.3.3 3rd Validation Experiment

In the last experiment, all the three Euler angles of the end-effector of the robotic arm follow a monotonic motion profile.

To demonstrate the performance of the attitude estimation algorithm presented in this paper, the estimation results from a quaternion based UKF algorithm in [13] is also shown. To make the estimation results comparable, the estimated quaternion is transformed to DCM by using standard equations [7]. The estimation results of all the three validation experiments can be seen in Fig. 7, 8 and 9 respectively. Each subplot in these figures shows each element of the DCM, where the index of the subplot corresponds to the element with same index in the matrix. The green solid line is the DCM computed form all the encoders data. The magenta dash line and the blue dot line represent the DCM estimated from the 9-axis motion sensor data by using the algorithm of this paper (labeled as algorithm 1) and [13] (labeled as algorithm 2) respectively.

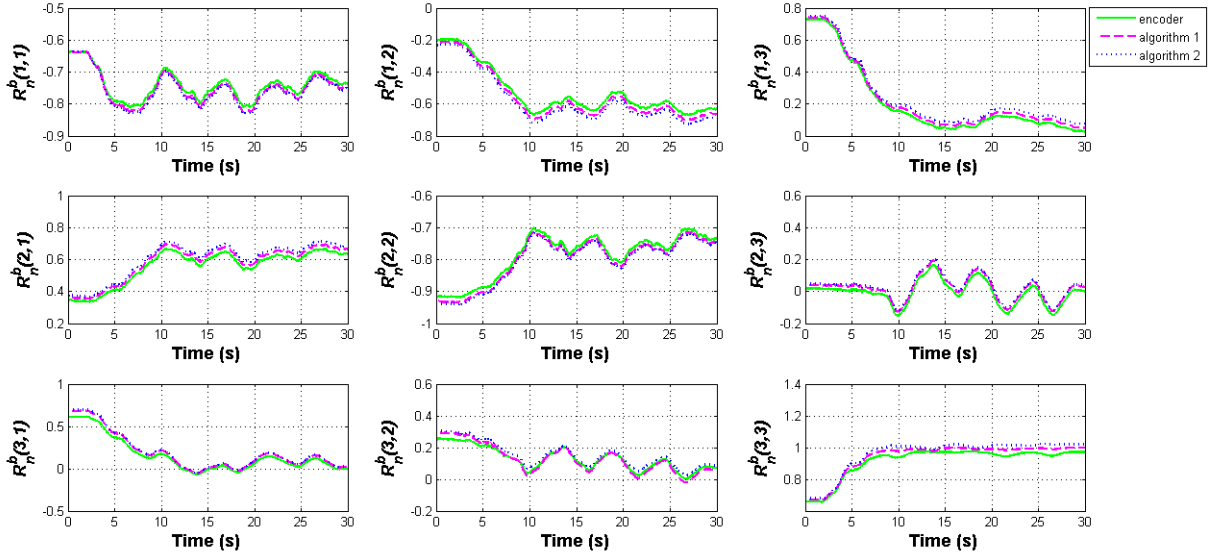


Fig. 8. The DCM estimation results in the second experiment

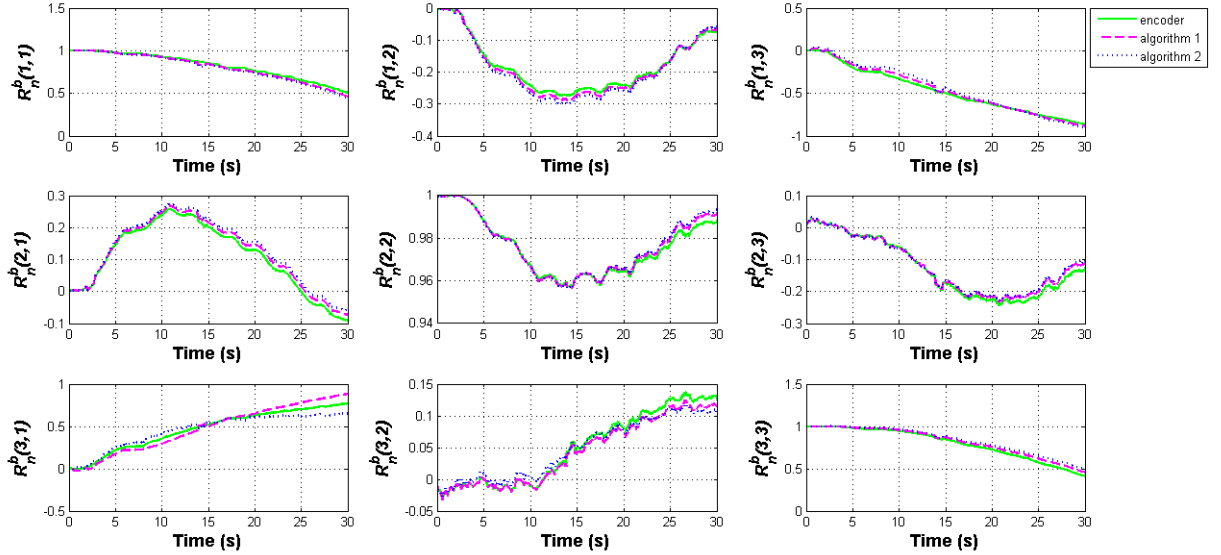


Fig. 9. The DCM estimation results in the third experiment

5.4 Estimation Error Analysis

As can be seen from Fig. 7, 8 and 9 that the estimated DCM matches the one from the encoders data in a good accuracy in all the three experiments. However, the estimation error is unavoidable in some plots. The following three factors contribute most to the estimation error.

- (1) Although the robotic arm is excited slowly, the centripetal acceleration of the end-effector exists but is not considered in the estimation algorithm.
- (2) Some plots show that there exists initial mismatch between the motion sensor and encoders.
- (3) The motion sensor has low resolution in some regions in the joint angle space due to the trigonometry functions in the DCM.

A comparison of the root mean square (RMS) of the estimation error of the algorithm from this paper (algorithm 1) with the one from [13] (algorithm 2) in all the three experiments is shown in Table below. It is quite clear that a better accuracy is achieved by the estimation algorithm presented in this paper.

		RMS of The Estimation Error		
		exp 1	exp 2	exp 3
$R_n^b(1, 1)$	algorithm 1	0.0099	0.0057	0.0099
	algorithm 2	0.0198	0.0113	0.0198
$R_n^b(1, 2)$	algorithm 1	0.0092	0.0283	0.0074
	algorithm 2	0.0115	0.0226	0.0092
$R_n^b(1, 3)$	algorithm 1	0.0033	0.0197	0.0249
	algorithm 2	0.0033	0.0197	0.0249
$R_n^b(2, 1)$	algorithm 1	0.0052	0.0183	0.0088
	algorithm 2	0.0074	0.0261	0.0126
$R_n^b(2, 2)$	algorithm 1	0.0013	0.0051	0.0008
	algorithm 2	0.0033	0.0128	0.0016
$R_n^b(2, 3)$	algorithm 1	0.0019	0.0088	0.0035
	algorithm 2	0.0023	0.0259	0.0102
$R_n^b(3, 1)$	algorithm 1	0.0024	0.0085	0.1102
	algorithm 2	0.0110	0.0386	0.0546
$R_n^b(3, 2)$	algorithm 1	0.0030	0.0181	0.0076
	algorithm 2	0.0030	0.0282	0.0078
$R_n^b(3, 3)$	algorithm 1	0.0185	0.0202	0.0202
	algorithm 2	0.0240	0.0263	0.0262

6 CONCLUSIONS

This paper discussed the design of a new DCM based attitude estimation algorithm using a 9-axis MEMS based motion tracking sensor, which includes a tri-axis accelerometer, a tri-axis gyroscope and a tri-axis magnetometer. The kinematic model of the DCM was transformed into a linear-time varying state space form based on which a linear Kalman filter algorithm was developed. An automatic calibration method for the time-drifting bias in the tri-axis magnetometer was also proposed. Finally, the estimation results are validated on real experimental data collected from the Invensense's MPU9250, which is attached to the end-effector of a 5-DOF robotic arm. The comparison with the built-in encoder data shows that the developed algorithm provides rather accurate estimates of the DCM under various excitation trajectories.

7 ACKNOWLEDGMENTS

This work was supported in part by funding from the US National Science Foundation under Grant CMMI 1562006.

References

- [1] H. Fourati; N. Manamanni; L. Afilal and Y. Handrich (2011). Posture and body acceleration tracking by inertial and magnetic sensing - application in behavioral analysis of free-ranging animals. *Biomedical Signal Processing and Control*, 6(1):94–104, 2011.
- [2] K. D. Nguyen; I. M. Chen; Z. Luo; S. H. Yeo and H. B. L. Duh (2011). A wearable sensing system for tracking and monitoring of functional arm movement. *IEEE/ASME Transactions on Mechatronics*, 16(2):213–220, 2011.
- [3] H. Ren and P. Kazanzides (2012). Investigation of attitude tracking using an integrated inertial and magnetic navigation system for hand-held surgical instruments. *IEEE/ASME Transactions on Mechatronics*, 17(2):210–217, 2012.

- [4] H. Zhou and H. Hu (2008). Human motion tracking for rehabilitationa survey. *Biomedical Signal Processing and Control*, 3(1):1–18, 2008.
- [5] B. Wang; L. Yu; Z. Deng and M. Fu (2016). A particle filter-based matching algorithm with gravity sample vector for underwater gravity aided navigation. *IEEE/ASME Transactions on Mechatronics*, 21(3):1399–1408, 2016.
- [6] S. Liu; D. Xu; F. Liu; D. Zhang and Z. Zhang (2016). Relative pose estimation for alignment of long cylindrical components based on microscopic vision. *IEEE/ASME Transactions on Mechatronics*, 21(3):1388–1398, 2016.
- [7] F. L. Markley and J. L. Crassidis (2014). *Fundamentals of Spacecraft Attitude Determination and Control*. Springer, 1st edition, 2014.
- [8] J. L. Crassidis; F. L. Markley and Y. Cheng (2007). A survey of nonlinear attitude estimation methods. *Journal of Guidance, Control, and Dynamics*, 30(1):12–28, 2007.
- [9] H. Fourati; N. Manamanni; L. Afilal and Y. Handrich (2014). Complementary observer for body segments motion capturing by inertial and magnetic sensors. *IEEE/ASME Transactions on Mechatronics*, 19(1):149–157, 2014.
- [10] Z. Q. Zhang; X. L. Meng and J. K. Wu (2012). Quaternion-based kalman filter with vector selection for accurate orientation tracking. *IEEE Transactions on Instrumentation and Measurement*, 61(10):2817–2824, 2012.
- [11] S. O. H. Madgwick; A. J. L. Harrison and R. Vaidyanathan (2011). Estimation of imu and marg orientation using a gradient descent algorihm. In *2011 IEEE International Conference on Rehabilitation Robotics*, Zurich, Switzerland, 2011.
- [12] D. Roetenberg; P. J. Slycke and P. H. Veltink (2007). Ambulatory position and orientation tracking fusing magnetic and inertial sensing. *IEEE Transactions on Biomedical Engineering*, 54(5):883–890, 2007.
- [13] Jaw-Kuen Shiau and I-Chiang Wang (2013). Unscented kalman filtering for attitude determination using mems sensors. *Journal of Applied Science and Engineering*, 16(2):165–176, 2013.
- [14] W. Premerlani and P. Bizard (2009). Direction cosine matrix imu: Theory. 2009.
- [15] L. Wei and J. Wang (2013). Effective adaptive kalman filter for mems-imu/magnetometers integrated attitude and heading reference systems. *Journal of Navigation*, 66:99–113, 2013.
- [16] R. Mahony; T. Hamel and J. M. Pflimlin (2008). Nonlinear complementary filters on the special orthogonal group. *IEEE Transactions on Automatic Control*, 53(5):1203–1218, 2008.
- [17] M. W. Spong; S. Hutchinson and M. Vidyasagar (2005). *Robot Modeling and Control*. Wiley, 1st edition, 2005.
- [18] J. Ginsberg (2007). *Engineering Dynamics*. Cambridge University Press, Cambridge, UK, 3rd edition, 2007.
- [19] G. Cook (2011). *Mobile Robots: Navigation, Control and Remote Sensing*. Wiley-IEEE Press, 1st edition, 2011.
- [20] P.l D. Groves (2007). *Principles of GNSS, Inertial, and Multi-Sensor Integrated Navigation Systems*. Artech House, 1st edition, 2009.
- [21] R. A. Johnson and D. W. Wichern (2007). *Applied Multivariate Statistical Analysis*. Pearson, 6th edition, 2007.
- [22] F. L. Lewis; L. Xie and D. Popa (2007). *Optimal and Robust Estimation: With an Introduction to Stochastic Control Theory*. CRC Press, 2nd edition, 2007.
- [23] P. Antsaklis and A. N. Michel (2007). *A Linear Systems Primer*. Birkhäuser Science, New York, USA, 2007.
- [24] R. M. Murray; Z. Li and S. S. Sastry (1994). *A Mathematical Introduction to Robotic Manipulation*. CRC Press, 1st edition, 1994.
- [25] T. Kailath; Ali H. Sayed and B. Hassibi (2000). *Linear Estimation*. Pearson, 1st edition, 2000.
- [26] D. Simon (2006). *Optimal State Estimation*. John Wiley & Sons, Hoboken, NJ, USA, 1st edition, 2006.
- [27] A. H. J. de Ruiter and J. R. Forbes (2017). Discrete-time $so(n)$ -constrained kalman filtering. *Journal of Guidance, Control and Dynamics*, 40(1):28–37, 2017.
- [28] G. Strang (2005). *Linear Algebra and Its Applications*. Brooks Cole, 4th edition, 2005.
- [29] R. N. Jazar (2010). *Theory of Applied Robotics: Kinematics, Dynamics, and Control*. Springer, 1st edition, 2010.